Vol 17 No 10, October 2008
1674-1056/2008/17(10)/3880-14

Chinese Physics B

© 2008 Chin. Phys. Soc.
and IOP Publishing Ltd

Surface plasmon polariton and mode transformation in a nanoscale lossy metallic cylindrical cable*

Yang Peng-Fei(杨鹏飞), Gu Ying(古 英)†, and Gong Qi-Huang(龚旗煌)‡

State Key Laboratory for Mesoscopic Physics, Department of Physics, Peking University, Beijing 100871, *China*

(Received 3 April 2008; revised manuscript received 13 May 2008)

A theoretical investigation on the surface plasmon polariton in a gold cylindrical nanocable is presented. By solving a complete set of Maxwell's equations in the nanocable (with a 50 nm radius gold nanocore, 10–300 nm silica layer, and 30–200 nm gold nanocladding), the dispersion relations on the optical frequency and on the silica thickness are discussed. When the silica thickness varies from 50 to 250 nm, at a fixed wavelength, the strong coupling between the gold nanocore and the nanocladding leads to a symmetric-like surface mode and an antisymmetric-like surface mode in the nanocable. The transformation between the surface mode and the waveguide mode in this structure is also investigated. The results will be helpful for understanding the surface waves in the subwavelength structures.

Keywords: nanocable, surface plasmons, mode transformation
PACC: 7320M, 4280L

1. Introduction

Surface plasmon polaritons (SPPs) are elementary excitations of the interaction system with collective oscillating electron gas and electromagnetic field.[1,2] In noble metals, the optical response is characterized by an effective dielectric constant from the phenomenological macroscopic treatment.[3,4] The surface wave modes in the subwavelength structures are then determined by solving the Maxwell's equations with certain boundary conditions. The electromagnetic field of this elementary excitation is bound to the interface. SPP, as an evanescent wave, can persist in the subwavelength scale. This feature opens up possibilities for using SPP as a signal carrier for the nanophotonic devices and interconnects.[5]

To channel the SPP, many subwavelength plasmonic waveguide structures have been proposed, such as thin metal films,[6] metal-insulator-metal slot structures,[7] metal stripe line,[8] groove on a metallic layer,[9] etc. The SPP propagation in the cylindrical waveguides with negative dielectric constants has been discussed by several authors. By using light scattering to excite SPP, the first experiment in a cylindrical aluminium wire was performed.[10] Subsequently, the results were explained by means of virtual radiative modes with a complex frequency.[11] The concentric two layer waveguide structures with one metallic layer have been thoroughly investigated by Prade and Vinet.[12] The lossy cylindrical metallic nanotubes with a dielectric core were used to model a probe of scanning near-field optical microscope (SNOM), and the transformation between the surface modes and waveguide modes has been reported.[13] In the study of a lossless cylindrical metallic nanotube, Schröter and Dereux[14] attributed the detection of a signal proportional to the magnetic field distribution in SNOM tips to the excitation of cylindrical SPPs. Recently, it is reported that a nanometric coaxial waveguide structure with two metal domains has a large cutoff wavelength and a reasonable large SPP propagation length.[15]

In the millimetre scale, electrical cables are widely used to transmit radio and microwave signals. For these spectral domains, the metals are very close to the perfect electric conductors. While, at the optical frequencies, the collective oscillation of free electrons in metal leads to a negative complex dielectric constant, which opens up possibilities for exciting SPP modes. In this paper, we will study the cylindrical nanocable at the optical frequencies, where the ordinary optical waveguide modes should cut off and only the SPPs can survive. The considered cylindri-

*Project supported by the National Natural Science Foundation of China (Grant Nos 10674009, 10521002 and 10434020) and the National Key Development Program for Basic Research of China (Grant No 2007CB307001).
†E-mail: ygu@pku.edu.cn
‡E-mail: qhgong@pku.edu.cn

cal nanocable has a 50 nm radius gold nanocore, 10–300 nm silica layer, and 30–200 nm gold nanocladding as shown in Fig.1. By solving a complete set of Maxwell's equations numerically, the whole spectrum of the nanocable is investigated. The dispersion relations on the optical frequency and on the silica thickness are discussed. Near plasmon frequency, some surface modes bend back and become radiative modes, which may be caused by the finite damping of metal. When the silica thickness varies from 50 to 250 nm, at a fixed wavelength, the symmetric-like and antisymmetric-like electric field distributions of surface modes are found to be due to a strong coupling between SPPs originating from the gold nanocore and nanocladding. For the symmetric-like mode, there is a long SPP propagation length. We also investigate the transformation between the surface mode and waveguide mode. In the nanoscale cable, the surface modes and waveguide modes will have some shifts and modification compared with the nanotubes of the same size (without the nanocore). In this structure the mode transformation phenomena are also very complicated, yet the action of nanocore is obvious. The results will be helpful for understanding the surface waves in the subwavelength structures, and may give some enlightenment in the SNOM detection.

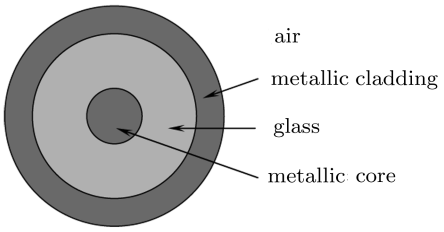


Fig.1. Schematic diagram of the nanocable structure.

The rest of the present paper is organized as follows. In Section 2, we outline the exact solution of Maxwell's equations under cylindrical boundary conditions by using the numerical method. In Section 3, the dispersion relations for the nanocable on the frequency and on the dielectric thickness, as well as the mode transformation phenomenon are discussed. Then in Section 4, the electromagnetic field distributions for $n = 0, 1$ modes are illustrated. The strong coupling region of SPPs is studied in detail. Finally, we summarize the main results in Section 5.

2. Theory

In this section, we briefly describe the theory and the numerical methods used in this work. The system under consideration is a cylindrical nanocable with metal, glass, metal, and air layers, as shown in Fig.1. The solution of Maxwell's equations in cylindrical structures is well documented in the textbook.[16] The electromagnetic fields of the eigenmodes in cylindrical coordinates (r, ϕ, z) have the following expressions (in Gauss units):[17]

$$
\begin{aligned}
E_r &= \left(\frac{\mathrm{i}k_z}{\gamma_j} f_n^{j\,\prime}(\gamma_j r) - \frac{\mu_j \omega n}{\gamma_j^2 r c} g_n^j(\gamma_j r)\right) \cdot S_n, \\
E_\phi &= \left(-\frac{n k_z}{\gamma_j^2 r} f_n^j(\gamma_j r) - \frac{\mathrm{i}\mu_j \omega}{\gamma_j c} g_n^{j\,\prime}(\gamma_j r)\right) \cdot S_n, \\
E_z &= f_n^j(\gamma_j r) \cdot S_n, \\
H_r &= \left(\frac{n\epsilon_j \omega}{\gamma_j^2 r c} f_n^j(\gamma_j r) + \frac{\mathrm{i}k_z}{\gamma_j} g_n^{j\,\prime}(\gamma_j r)\right) \cdot S_n, \\
H_\phi &= \left(\frac{\mathrm{i}\epsilon_j \omega}{\gamma_j c} f_n^{j\,\prime}(\gamma_j r) - \frac{n k_z}{\gamma_j^2 r} g_n^j(\gamma_j r)\right) \cdot S_n,
\end{aligned}
$$

and

$$
H_z = g_n^j(\gamma_j r) \cdot S_n, \tag{1}
$$

where i is the imaginary unit, n an integer ($n = 0, 1, 2, \ldots$), k_z the propagation constant, and ϵ_j the dielectric function of the medium j. The propagation constant k_z is complex due to the loss of metal. The real part of k_z is the phase constant and the imaginary part of k_z is the attenuation constant. The index j denotes that c = core, d = dielectric (glass layer), m = metal cladding layer, and a = air. As we are not to deal with magnetic materials, the magnetic permeability μ is considered to be unity everywhere. S_n is the exponential factor, and γ_j is the transverse wave number in the jth medium; they are expressed as

$$
S_n = \exp(\mathrm{i}n\phi + \mathrm{i}k_z z - \mathrm{i}\omega t),
$$

and

$$
\gamma_j^2 = \mu_j \epsilon_j (\omega/c)^2 - k_z^2 \tag{2}
$$

where c is the speed of light in vacuum. The radial dependent functions f_n^j and g_n^j are solutions of Bessel's equation. Generally, f_n^j and g_n^j are the superposition of Bessel functions. In the inner core domain only a Bessel function of the first kind, J_n, can be used in order to have a finite solution when $r \to 0$. For the outermost domain, only a Hankel function of the first

kind, $H_n^{(1)}$, can be applied and the value of γ_j with a positive imaginary part must always be taken in order to fulfil the radiation condition at infinity.[18] In the closed domain between the inner core and the outermost air, f_n^j and g_n^j are linear superposition of the first and second kind Bessel functions J_n and Y_n. In each case $f_n^{j\prime}(x)$ and $g_n^{j\prime}(x)$ denote the derivative of $f_n^j(x)$ and $g_n^j(x)$ with respect to its argument x, respectively.

By applying the boundary conditions that the tangential components of the electric and the magnetic fields must be continuous at the interface, a homogeneous system of linear equations satisfied by the expansion coefficients of f_n^j and g_n^j by Bessel functions is obtained. The existence of the nontrivial solutions is guaranteed by letting the determinant of the system vanish, then we obtain the following transcendental equation:

$$\det[M(k_z)] = 0 \tag{3}$$

for the complex propagation constant k_z. M is the resulting matrix of the linear system of equations. For a nanocable with 4 layers, there are 12 coefficients and the size of this matrix is therefore 12. For order $n = 0$ the matrix can be split into two independent 6 order submatrices corresponding to TE and TM solutions.[13] The determinant is complex and Eq.(3) must be fulfilled for real and imaginary parts simultaneously. So Eq.(3) is equivalent to $|\det[M(k_z)]| = 0$, which can be used as another criterion for the determination of k_z.

We have used two independent algorithms to solve the transcendental equation. In the first one we adopted an algorithm following the procedure in Ref.[13]. Firstly, we divided the finite area in which we search for solutions into $n \times n (n \sim 10^4)$ subareas. And the $|\det[M(k_z)]|$ values on each grid were calculated and compared. The average value of $|\det[M(k_z)]|$ over all grids was computed simultaneously. If the value of $|\det[M(k_z)]|$ on a certain grid is less than those on surrounding grids, there must exist a minimum around that grid. Secondly, we wrote an code to search for minimum in the surrounding areas. If the minimum found in the second step was 15 orders of magnitude smaller than the average value of $|\det[M(k_z)]|$, then it was identified as a mode. In the second algorithm we used a mathematic software package to find the zero points of an analytic function in the complex plane.[19] The results of two procedures are in good agreement with each other.

In this paper, the metal in the core and cladding is gold, and its frequency-dependent dielectric-constant is taken from the experimental handbook.[20] The loss of metal is considered and the attenuation is associated with the imaginary part of the complex dielectric constant. The dielectric constant of glass, ϵ_{glass}, is 2.0.

3. Dispersion relations

In this section, various mode dispersion relations are investigated. First, we give the mode classification and nomenclature rules, then the mode dispersion relation curves on frequency and dielectric thickness are plotted and the mode transformation is discussed. For each n, there may exist many solutions to Eq.(3). Each solution corresponds to an eigenmode of the nanocable. In the following, the index n denotes the angular symmetry of the mode and the index m represents the radial dependence of the field. In a cylindrical waveguide, the $n = 0$ modes are either transverse magnetic or transverse electric, which are named TM_{0m} or TE_{0m} respectively. For $n > 0$, the modes are generally hybrid, which have nonzero values for both E_z and H_z. Nevertheless, these modes are often TM dominated or TE dominated, so they are designated EH_{nm} modes or HE_{nm} modes respectively. For a single interface cylindrical waveguide, such as a nanowire, there is a definite classification about EH and HE modes.[21] While for a multi-interface cylindrical waveguide structure, such as nanotube or nanocable, there are no rigorous definitions about EH and HE modes. In this paper, referring to Ref.[13], we distinguish EH mode from HE mode by comparing the amplitudes of E_z and H_z. If $|E_z| > |H_z|$, then this mode is regarded as TM-like and designated as an EH mode; if $|E_z| < |H_z|$, this mode is regarded as TE-like and designated as an HE mode. The adoption of this designation is only for the convenience of modes citing, and it is somewhat arbitrary. In the nanocable, the behaviours of modes are very complex and strongly dependent on the material properties and geometric parameters.

3.1. Mode dependence on frequency

In this section, we investigate the mode dependence on frequency in nanocables. The frequency range we investigate is 0.6–6 eV(λ = 2000–200 nm), which is from far-infrared to ultra-violet. The frequency dependent dielectric constant of gold is taken from experimental data.[20] To obtain smooth disper-

sion curves, the experimental data are interpolated in some frequency range. The dielectric constant of glass is always taken to be 2.0.

In Figs.2 and 3, TM_{01} and TM_{02} modes of nanocable varying with frequency are plotted. At low frequencies, TM_{01} modes tend to the light line of glass, while TM_{02} modes tend to the light line of vacuum. This can be explained as follows. When the frequency is small, gold behaves like a perfect conduct due to the large dielectric constant (for example, at $\lambda = 2000\,\mathrm{nm}$, the dielectric constant of gold is $-158.04 + \mathrm{i}21.4$). Then the electromagnetic field mainly distributes within the glass and air, thus the loss of electromagnetic field is very small. The TM_{01} modes lie below the glass light line and are surface modes. While the TM_{02} modes lie between the glass light line and the vacuum light line, and they are non-radiative waveguide modes. Below the frequency $2.4\,\mathrm{eV}(\lambda = 516.6\,\mathrm{nm})$, the real and the imaginary parts of two modes increase with frequency. When $\omega > 2.7\,\mathrm{eV}$, with the increase of frequency, some TM_{01} modes cross the glass light line and transform into non-radiative waveguide modes. The TM_{02} mode with $D_1 = 100\,\mathrm{nm}$ first crosses the air light line and turns into a waveguide mode, and then crosses the air light line again and transforms into a non-radiative mode. All TM_{02} modes lie between the glass light line and the air light line, and so they are the non-radiative modes. When the frequency becomes very large, the loss of gold increases rapidly (for example, when $\omega = 3.1\,\mathrm{eV}$, $\epsilon_{\mathrm{gold}} = -1.077 + \mathrm{i}6.486$ and $\mathrm{Im}[\epsilon_{\mathrm{gold}}] \gg \mathrm{Re}[\epsilon_{\mathrm{gold}}]$). For the same frequency, the real part $\mathrm{Re}[k_z]$ of TM_{01} mode with $D_1 = 50\,\mathrm{nm}$ has a larger value than that with $D_1 = 100\,\mathrm{nm}$ or $200\,\mathrm{nm}$.

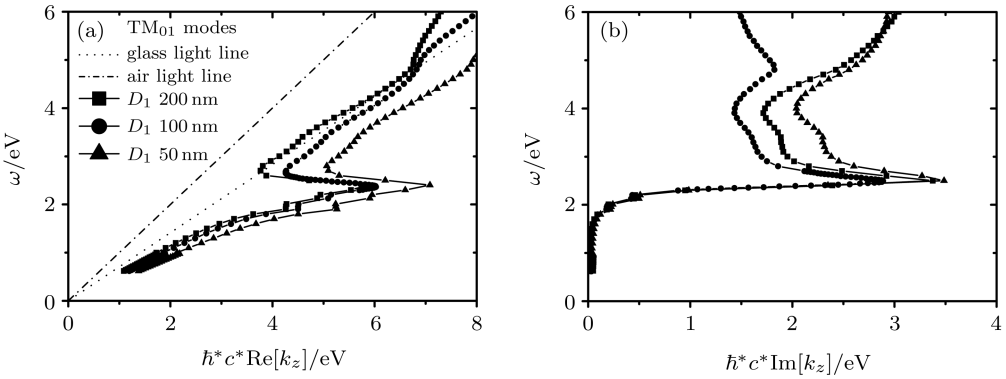


Fig.2. Frequency dispersion of the TM_{01} mode for different values of dielectric thickness D_1, with core radius $R_0 = 50\,\mathrm{nm}$ and cladding thickness $D_2 = 30\,\mathrm{nm}$.

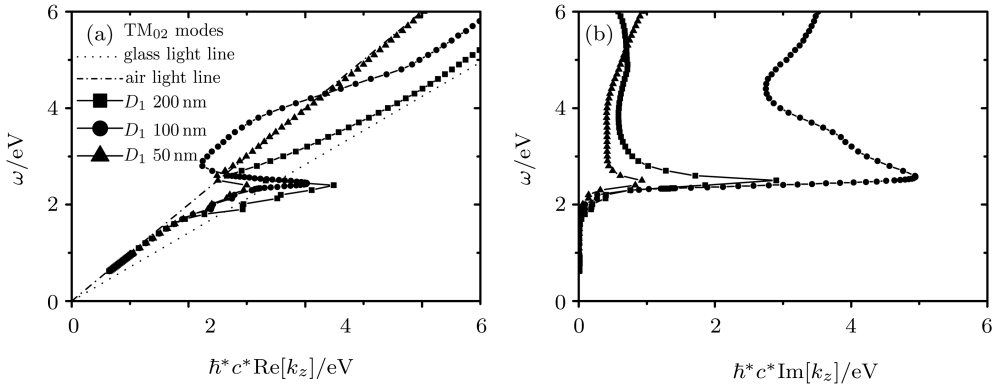


Fig.3. Frequency dispersion of the TM_{02} mode for different values of dielectric thickness D_1, with core radius $R_0 = 50\,\mathrm{nm}$ and cladding thickness $D_2 = 30\,\mathrm{nm}$.

Now we focus on the behaviours near the gold plasmon frequency 2.4 eV. In Figs.2 and 3, it is seen that the real parts of propagation constants of TM_{01} and TM_{02} modes can arrive at a maximum. These maxima have the same position and are independent of D_1. Simultaneously, the imaginary parts of two modes increase suddenly and arrive at a maximum at $\omega = 2.5\,\mathrm{eV}(\lambda = 495.9\,\mathrm{nm})$. Then both the real and the imaginary parts of the propagation constants start to decrease. For TM_{01}, $\mathrm{Re}[k_z]$ reaches a minimum at

$\omega \approx 2.7\,\mathrm{eV}(\lambda \approx 459.2\,\mathrm{nm})$; while, for TM_{02}, $\mathrm{Re}[k_z]$ reaches a minimum at $\omega \approx 2.6\,\mathrm{eV}(\lambda \approx 476.9\,\mathrm{nm})$. In other waveguide structures, such as lossless metallic surface[1] or metallic coaxial waveguide,[15] the propagation constant tends to infinity near plasmon frequency and there is a gap between surface plasmon modes and radiative modes; while for a lossy nanocable waveguide, the TM modes transform from surface modes into radiative modes continuously near the plasmon frequency. This backbending phenomenon has also been reported experimentally in an air-metal interface[22] and theoretically in the lossy metallic nanowire and nanotube.[13] The dispersion curves for surface electromagnetic waves with damping has been investigated by Alexander *et al.*[23] They proved that whether or not the dispersion curve exhibits backbending is related to the details of experiment and method used to obtain the results. In Section 4, the electromagnetic field distributions of TM modes with different frequencies are plotted to display the feature of modes.

In Figs.4 and 5, the frequency dispersion curves of EH_{11} and EH_{12} modes are plotted. The behaviour of EH_{11} modes is similar to that of TM_{02} modes, i.e. they tend to the vacuum light line at small frequencies, reach a maximum near plasmon frequency, and turns into the radiative modes continuously. At small frequencies, the dispersion curves of EH_{12} first cross the vacuum light line and turn into the radiative modes, then cut off with a large loss. This phenomenon has also been observed for the $n = 1$ surface plasmon modes in lossless metallic coaxial waveguides.[15]

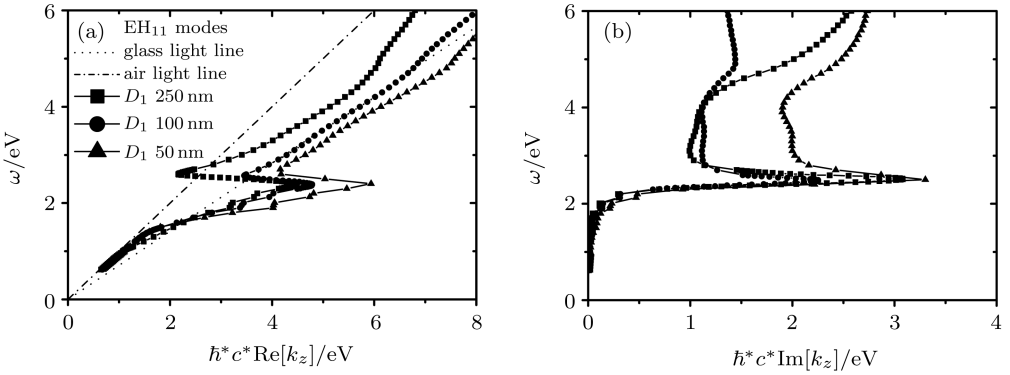


Fig.4. Frequency dispersion of the EH_{11} mode for different values of dielectric thickness D_1, with core radius $R_0 = 50\,\mathrm{nm}$ and cladding thickness $D_2 = 30\,\mathrm{nm}$.

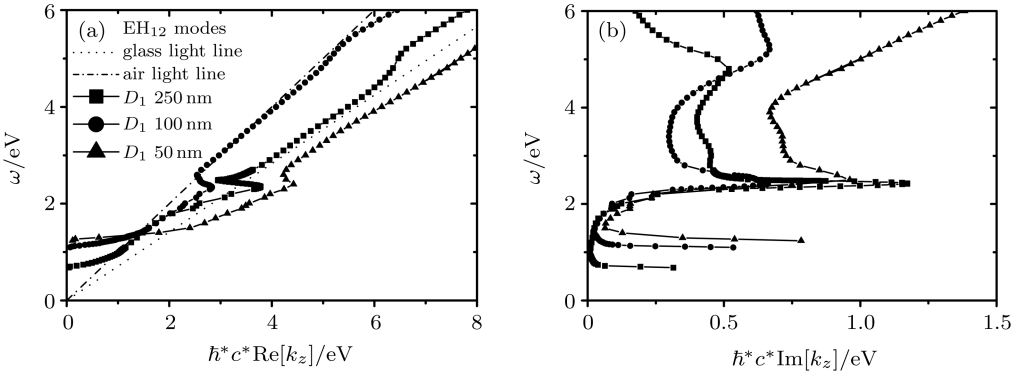


Fig.5. Frequency dispersion of the EH_{12} mode for different values of dielectric thickness D_1, with core radius $R_0 = 50\,\mathrm{nm}$ and cladding thickness $D_2 = 30\,\mathrm{nm}$.

3.2. Mode dependence on dielectric thickness

Now we investigate the mode dependence of gold nanocable on the thickness of dielectric layer. The light wavelength in free space is fixed at 632.8 nm. At this frequency, the dielectric constant of gold is $\epsilon_{\mathrm{gold}} = -10.33 + \mathrm{i}1.19$.[20] The gold nanocore radius and the thickness of gold nanocladding are chosen be to 50 nm and 30–100 nm. Dielectric thickness D_1 varies from zero to 350 nm. Figures 6–8 show the real and the imaginary parts of propagation constant k_z

for $n = 0, 1, 2$ as a function of dielectric thickness D_1. For comparison, the results of the 50 nm radius gold nanowires and the gold nanotubes with a 30 nm thick gold nanocladding are also illustrated. For nanotubes, the abscissa represents the core radius R_0.

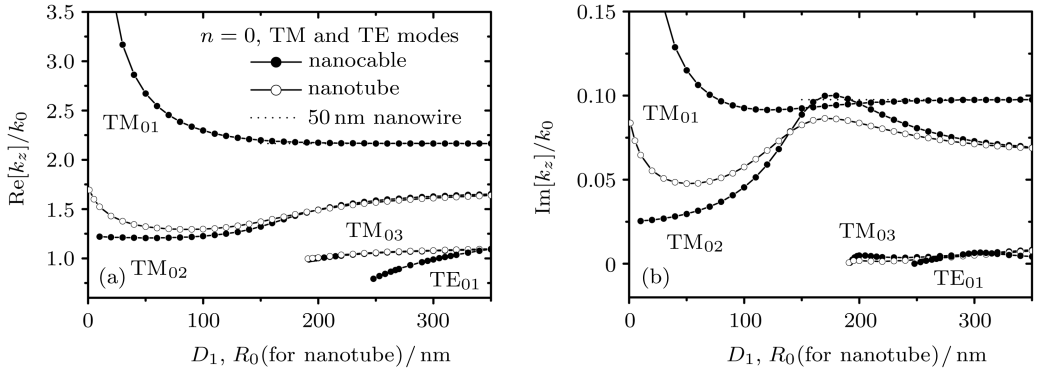


Fig.6. Propagation constants of the $n = 0$ modes as a function of D_1 (for nanocable) or R_0 (for nanotube). Wavelength $\lambda = 632.8$ nm. Here $\epsilon_{gold} = -10.3 + \mathrm{i}1.2$ and $\epsilon_{\mathrm{glass}} = 2.0$. The gold nanocore radius is 50 nm and the gold nanocladding is 30 nm.

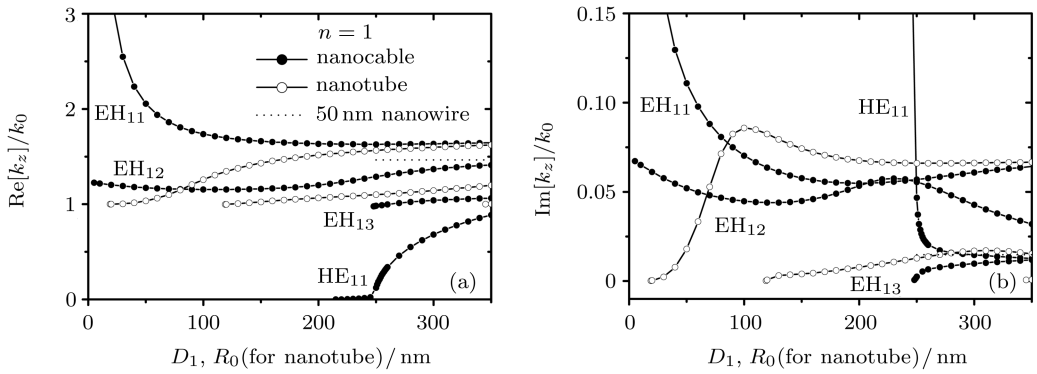


Fig.7. Propagation constants of the $n = 1$ modes as a function of D_1 (for nanocable) or R_0 (for nanotube). The same parameters are used as those in Fig.6.

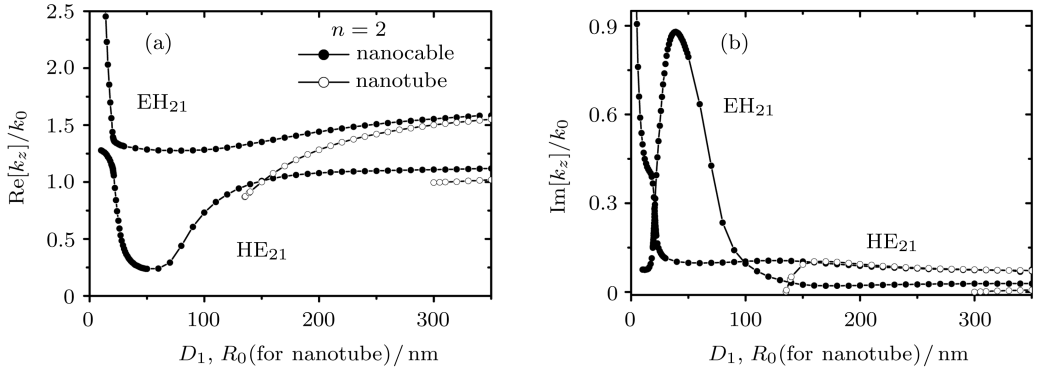


Fig.8. Propagation constants of the $n = 2$ modes as a function of D_1 (for nanocable) or R_0 (for nanotube). The EH_{21} surface mode transforms into the HE_{21} evanescent mode and vice versa. The same parameters are used as those in Fig.6.

In Fig.6, the propagation constants of TM and TE modes for $n = 0$ are plotted with D_1 changing from 0 to 350 nm. For a lossless cylindrical waveguide, since the transverse wave numbers are either real or purely imaginary, the electromagnetic fields of these modes are either oscillating or evanescent along the radial direction. While for a lossy nanocable, since the propagation constant k_z and transverse wave num-

ber are generally complex, the modes are more or less evanescent. If the transverse wave number is close to the real or the imaginary axis, we may still take it as an oscillating or evanescent mode. For the TM_{01} and TM_{02} modes, they are evanescent modes in the radial direction in all domains. For the TM_{03} mode, $\sqrt{\epsilon_{\rm glass}}k_0 > {\rm Re}[k_z] > k_0$, this mode is oscillating in the glass layer and evanescent in other domains. The lowest TM_{03} mode is cutoff at $D_1 \approx 190\,{\rm nm}$. The cutoff condition is expressed as[13]

$$\mathrm{Im}[k_{\rm air}] = 0, \tag{4}$$

which can be fulfilled if

$$\mathrm{Re}[k_z] = 0, \tag{5}$$

or

$$\mathrm{Im}[k_z] = 0 \qquad \text{and} \qquad 0 < \mathrm{Re}[k_z] < k_0. \tag{6}$$

For a 30 nm radius gold nanotube, almost the same cutoff radius is found. The curves from up to down in Fig.6(a) correspond to the three TM modes of nanocables, i.e. the antisymmetric-like surface mode, symmetric-like surface mode, non-radiative waveguide mode respectively (see the details of the electromagnetic field distribution in the next section). Finally, TE_{01} is also a non-radiative mode.

The attenuation of electromagnetic fields in a nanocable is caused by the thermal loss of metal and radiative loss. For surface modes, the main source of attenuation is thermal loss, which is proportional to the electric field intensity in metal. For TM_{03} and TE_{01} modes, the electromagnetic fields mainly distribute in the glass layer, thus the loss is very small ($\mathrm{Im}[k_z]/k_0 \approx 10^{-2}$), as shown in Fig.6(b). The propagation lengths of these two modes each are about $60\,\mu$m. For TM_{01} and TM_{02} modes, the electromagnetic fields are located in the vicinity of metal-dielectric interface, so the losses of these two modes are much larger ($\mathrm{Im}[k_z]/k_0 \approx 10^{-1}$) and the propagation lengths each are about $10\,\mu$m. The electromagnetic field distributions of TM_{01} and TM_{02} modes are very similar to the antisymmetric and symmetric surface modes of a plane metal-insulator-metal waveguide structure.[7] In the glass layer, E_z changes its sign for TM_{01} mode, while it keeps the sign unchanged for TM_{02} mode (see details in the next section). The proportion of electric field of TM_{01} mode distributed in glass layer is less than that of TM_{02} mode, thus the loss of TM_{01} mode is larger than that of TM_{02} mode. For TM_{02} mode, there is a broad maximum near $D_1 = 180\,{\rm nm}$ in the $\mathrm{Im}[k_z]$ curve, which is caused by the coupling between TM_{02} and TM_{03} modes (see the detailed explanation in mode transformation subsection).

For comparison, the propagation constants of TM modes of 30 nm radius gold nanotube (blue circles) and TM surface mode of 50 nm radius gold nanowire embedded in an infinite glass cladding (dotted line) are also shown in Fig.6. We observe that, for a large D_1, the TM_{01} mode tends to the TM surface mode of 50 nm radius nanowire,[13] and both the TM_{02} and the TM_{03} tend to the TM modes of 30 nm radius gold nanotube.[13] And when D_1 is large enough, two TM modes will approach to the result of 30 nm thick planar gold film.[6] This behaviour is explained as follows. The nanocable may be regarded as a compound of a 50 nm radius nanowire core and a 30 nm radius gold nanotube. When the dielectric thickness is large, the coupling between the core and cladding is weak, then the modes of nanocable tend to the modes of nanowire or nanotube. On the other hand, when D_1 decreases to zero, the real and the imaginary parts of the propagation constants of TM_{01} mode tend to infinity, and the results of TM_{02} mode tend to the surface modes of 80 nm radius gold nanowire.[13]

Figure 7 displays the propagation constants of the lowest four $n = 1$ modes for the gold nanocables, as well as the lowest three $n = 1$ modes for the gold nanotubes and the $n = 1$ surface mode for 50 nm radius gold nanowire embedded in an infinite glass domain. The features of the upper three $n = 1$ modes are very similar to those of the TM modes. For EH_{11} and EH_{12} modes, they are the evanescent modes in the radial direction in all domains. While, for the EH_{13} mode, $\sqrt{\epsilon_{\rm glass}}k_0 > {\rm Re}[k_z] > k_0$, it is an oscillating mode in the glass layer but it is an evanescent mode in the other domains. For the HE_{11} mode, $\mathrm{Re}[k_z] < k_0$ when $D_1 < 350\,{\rm nm}$, this mode is oscillating in the glass layer and radiative along the radial direction. From up to down, the four modes are an antisymmetric-like surface mode, a symmetric-like surface mode, a non-radiative waveguide mode, and a radiative waveguide mode, sequentially. At a large D_1, the symmetric-like EH_{11} mode tends to the surface mode of gold nanotube;[13] while the antisymmetric-like EH_{12} mode tends to the $n = 1$ surface mode of 50 nm radius gold nanowire.[13] This asymptotic behaviour is different from that of the corresponding TM modes. When D_1 decreases, the phase constant of HE_{11} mode decreases toward zero, while the attenuation constant increases

drastically. It means that a waveguide mode transforms into an radiative mode, and simultaneously the radiative loss becomes very large. At $D_1 \approx 230\,\mathrm{nm}$, the phase constant of HE_{11} comes to zero and immediately is cutoff because of the condition of expression (5). The EH_{13} mode is cutoff at $D_1 \approx 250\,\mathrm{nm}$ due to the condition of expression (6). At the limit $D_1 \to 0$, the EH_{12} mode tends to the $n = 1$ surface mode of 80 nm radius gold nanowire embedded in vacuum,[13] while the propagation constant of EH_{11} mode tends to infinity.

For $n = 1$ mode, the attenuation of three EH modes is mainly caused by thermal loss. As shown in Fig.7(b), for EH_{13} mode the electromagnetic fields mainly distribute in the glass layer and the loss is very small ($\mathrm{Im}[k_z]/k_0 \approx 10^{-2}$). The propagation length of this mode is about $60\,\mu\mathrm{m}$. EH_{11} mode is antisymmetric-like while EH_{12} is symmetric-like. The proportion of electric field distribution in metal of EH_{11} mode is larger than that of EH_{12} mode, thus the loss of EH_{11} mode is larger than that of EH_{12} mode in most cases. When D_1 decreases to zero, the loss of EH_{11} mode tends to infinity, and the electric fields of EH_{12} mode transfer to the outer metal-air interface. In this case, the loss of EH_{12} mode decreases to that of the $n = 1$ surface mode of 80 nm radius gold nanowire.[13] For the EH_{12} mode, there is a maximum near $D_1 = 230\,\mathrm{nm}$ in the $\mathrm{Im}[k_z]$ curve, this peak is also caused by the coupling between EH_{12} and EH_{13} (see detailed explanation in the next subsection).

In Fig.8, the propagation constants of $n = 2$ modes of gold nanocable and nanotube are plotted. When $D_1 < 350\,\mathrm{nm}$, EH and HE modes are found for both nanocable and nanotube. The $n = 2$ surface mode is cutoff in the 50 nm radius gold nanowire. When $D_1 > 150\,\mathrm{nm}$, $\mathrm{Re}[k_z] > \sqrt{\epsilon_{\mathrm{glass}}}k_0$ for EH_{21} mode and $\sqrt{\epsilon_{\mathrm{glass}}}k_0 > \mathrm{Re}[k_z] > k_0$ for HE_{21} mode. EH_{21} mode is an evanescent mode in the radial direction in all domains and HE_{21} mode is evanescent in the outmost air domain while oscillating in the glass layer. When D_1 decreases to 100 nm, the phase constant of HE_{21} mode decreases while the attenuation constant increases sharply. HE_{21} mode transforms into a radiative mode. At $D_1 \approx 50\,\mathrm{nm}$, the phase constant of HE_{21} mode arrives at a minimum while the attenuation constant reaches a maximum. At $D_1 \approx 20\,\mathrm{nm}$, both the phase constant and the attenuation constant of EH_{21} mode increase sharply. In this case, the propagation constants of EH_{21} and HE_{21} modes come close to each other in a complex plane, and the strange behaviours of two modes are caused by the strong coupling between them (see the details in the next subsection). When $D_1 \to 0$ the propagation constant of HE_{21} mode tends to a finite value, while the propagation constant of EH_{21} mode tends to infinity. On the other hand, when D_1 is large enough ($\approx 300\,\mathrm{nm}$), these modes tend to the modes of a planar gold film embedded in the semi-infinite glass and air.[1] We also observe that two nanotube modes cut off at 300 nm and 135 nm. For the HE_{21} mode, there is a maximum near $D_1 = 50\,\mathrm{nm}$ in the $\mathrm{Im}[k_z]$ curve, this peak is caused by transformation between EH_{21} and HE_{21} modes (see detailed explanation in the next subsection).

3.3. Mode transformation

In the dispersion curves of nanocable, we have observed an interesting mode transformation phenomenon. It is known that in the cylindrical gold nanostructures the surface modes and waveguide modes coexist at certain parameters. In the nanocable, with the value of D_1 decreasing, generally the waveguide modes transform into evanescent modes and then become cutoff, and the phase constants $\mathrm{Re}[k_z]$ vary from $\sqrt{\epsilon_{\mathrm{glass}}}k_0$ to 0; while for some surface modes, the phase constants vary slightly with $D_1(\mathrm{Re}[k_z] \approx k_0)$. It looks as if in this process the $\mathrm{Re}[k_z]$ curves of these two modes must cross each other. Actually this crossing has been found in the following Figs.9(a) and 9(b) and Figs.10(a) and 10(b). The interesting thing is that when the $\mathrm{Im}[k_z]$ curves of these two modes come close to each other and the $\mathrm{Re}[k_z]$ curves show anticrossing behaviour, the mode transformation between these two modes occur. This mode transformation phenomenon was first reported in metallic nanotube in Ref.[11].

The mode transformation process for $n = 1$ is shown in Fig.9. For $D_2 = 120\,\mathrm{nm}$ (Figs.9(a) and 9(b)), the $\mathrm{Re}[k_z]$ curves of EH_{12} and HE_{11} modes cross each other near $D_1 = 260\,\mathrm{nm}$. The mode transformation does not happen. Nevertheless, the coupling between these two modes leads to a slight response in the $\mathrm{Im}[k_z]$ curves. When D_2 decreases, the coupling induced response in $\mathrm{Im}[k_z]$ curves becomes stronger. At $D_2 = 100\,\mathrm{nm}$ (Figs.9(c) and 9(d)), the $\mathrm{Im}[k_z]$ curves of EH_{12} and HE_{11} modes cross each other while the $\mathrm{Re}[k_z]$ curves avoid crossing (see the insets in Figs.9(c) and 9(d)). Then the surface mode transforms into waveguide mode and vice versa. When the value of

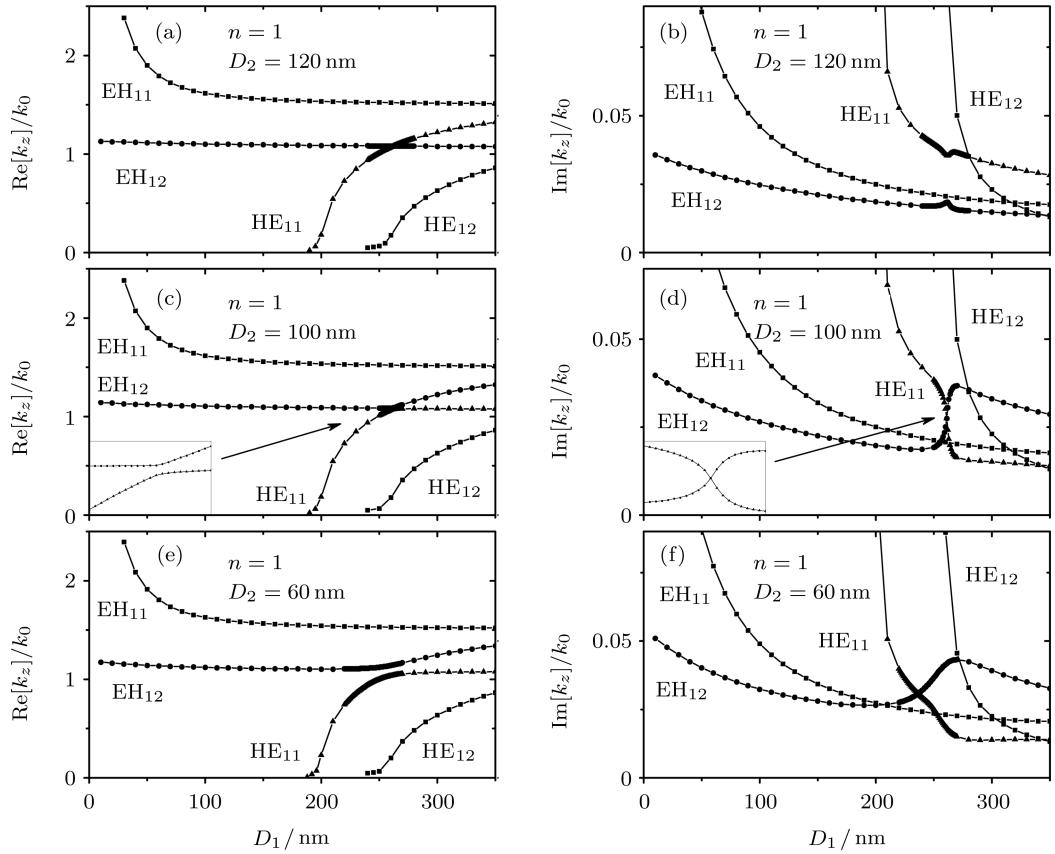


Fig.9. Propagation constants of the $n = 1$ modes as a function of D_1, with the values of gold cladding thickness D_2 being 120 (a), 100 (c) and 60 nm (e). The Re[k_z] curves of HE_{11} and EH_{11} modes are crossing in (a), anticrossing in (c), and after anticrossing in (e). The same parameters are used as those in Fig.7, except that the gold nanocladdings are different.

D_2 decreases further, such as for $D_2 = 60$ nm (Figs.9(e) and 9(f)), the Re[k_z] curves of EH_{12} and HE_{11} modes leave away from each other and become smooth, the transformation induced peak in the Im[k_z] curve of EH_{12} mode is broadened and the mode transformation becomes unnoticeable. At $D_2 = 30$ nm, the mode transformation is almost unobservable in Re[k_z] curves but the maximum in the Im[k_z] curve of EH_{12} mode still exists as shown in Fig.7. The maximum in the Im[k_z] curve of TM_{02} mode is also caused by the mode transformation. For $n = 1$, the Im[k_z] curves of EH_{12} and HE_{11} modes intersect only once in the transformation, which is a little different from the nanotube results,[13] where the Im[k_z] curves intersect twice. More numerical calculations indicate that for a nanotube where $D_2 = 100$ nm, mode transformation will happen near $R_0 = 120$ nm. While for a nanocable where $D_2 = 100$ nm, the mode transformation is at $D_1 = 260$ nm. The $n = 1$ mode transformation is greatly influenced by the 50 nm radius gold nanocore compared with the nanotube results.

Figure 10 displays the curves of $n = 2$ modes with different values of gold cladding thickness D_2. For $D_2 = 200$ nm (Figs.10(a) and 10(b)), the Re[k_z] curves of EH_{21} and HE_{21} modes cross each other at about $D_1 = 177$ nm, while the Im[k_z] curves cross each other at about $D_1 = 210$ nm. The mode transformation does not happen. When D_2 decreases, the cross point of the Re[k_z] curves of EH_{21} and HE_{21} modes moves to the right, while the cross point of the Im[k_z] curves moves to the left. When these two cross points meet, the mode transformation happens. For $D_2 = 100$ nm (Figs.10(c) and 10(d)), both the Re[k_z] and Im[k_z] curves come close to each other at about $D_1 = 181$ nm, then the surface mode transforms into a waveguide mode and vice versa. The Re[k_z] curves avoid crossing while the Im[k_z] curves cross twice. When D_2 decreases further, such as for $D_2 = 60$ nm (Figs.10(e) and 10(f)) or $D_2 = 30$ nm (Figs.8(a) and 8(b)), the Re[k_z] curves of EH_{21} and HE_{21} modes leave away from each other and become smooth, thus the mode transformation becomes

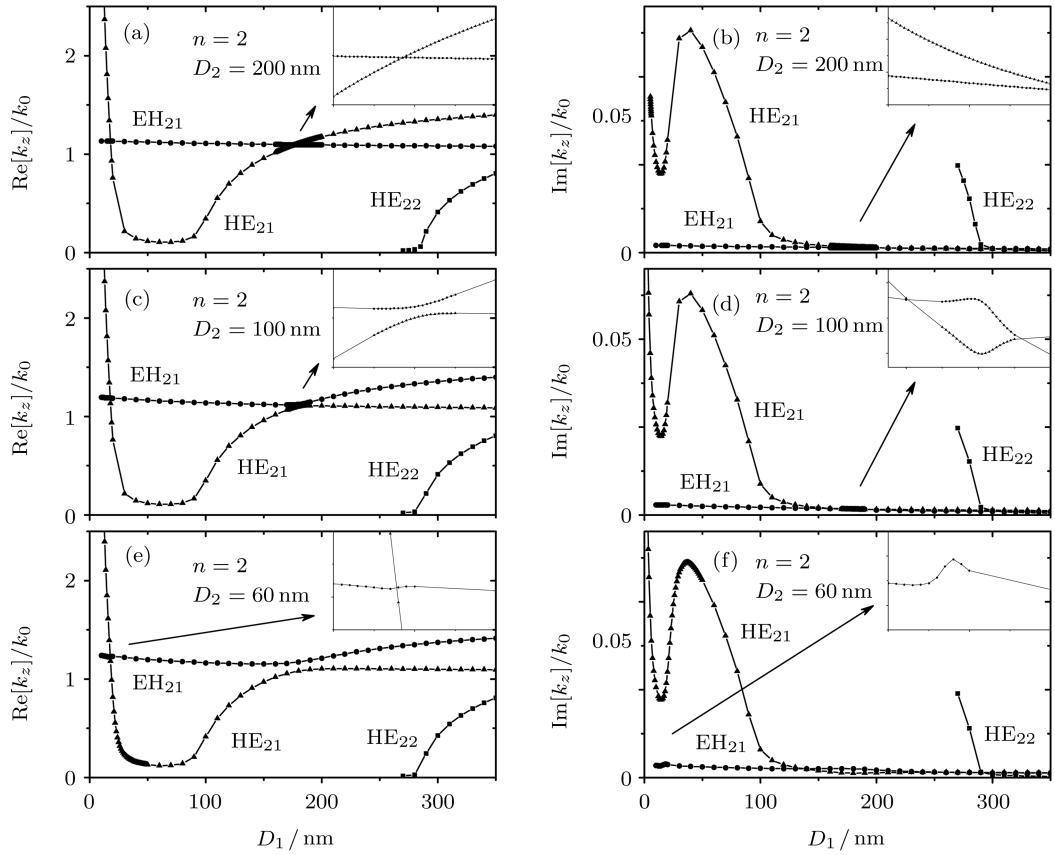


Fig.10. Propagation constants of the $n = 2$ modes as a function of D_1, with the values of gold cladding thickness D_2 being 200 (a), 100 (c) and 60 nm (e). The Re[k_z] curves of HE_{21} and EH_{21} modes are crossing in (a), anticrossing in (c) and after anticrossing in (e). The same parameters are used as those in Fig.8, except that the gold nanocladdings are different.

unnoticeable. When $D_1 \to 0$, both the Re[k_z] and the Im[k_z] curves of HE_{21} modes tend to infinity while the EH_{21} modes tend to a finite value. The Re[k_z] curves of these two modes cross at about $D_1 = 18$ nm, and the coupling between these two modes pulls down the Im[k_z] curves of HE_{21} modes and induces slight peaks in the Im[k_z] curves of EH_{21} modes near $D_1 = 18$ nm (see the inset in Fig.10(b)). With the value of D_2 decreasing, the peak in the Im[k_z] curve of EH_{21} mode becomes strong and mode transformation happens again when it touches the valley in the Im[k_z] curves of HE_{21} modes near $D_1 = 18$ nm. For example, for $D_2 = 30$ nm in Fig.8, the mode transformation between EH_{21} and HE_{21} modes happens near $D_1 = 18$ nm. The Re[k_z] curves anticross each other while the Im[k_z] curves cross once. After transformation, the Im[k_z] curve of EH_{21} mode tends to infinity while HE_{21} mode tends to a finite value, and a large peak is formed in the Im[k_z] curve of HE_{21} mode.

From the above cases, we have found that the mode transformation happens when the Re[k_z] and the Im[k_z] curves of two modes meet at almost the same point. The mode dependence on the parameters such as D_1, D_2, and frequency ω is very complicated, so it is not easy to judge whether the mode transformation happens or not by the given parameters. The influence of nanocore on the mode transformation is obvious, because in the nanotubes of the same size the behaviours of mode transformation are very different (the calculation details are not provided here).

4. Electromagnetic field distributions

To give an intuitionistic illustration, in this section, we investigate the electromagnetic field distribution of the surface modes of the nanocable. As mentioned in the previous section, the gold nanocable may be regarded as a combination of a gold nanotube and a gold nanowire, so the surface modes of nanocable may originate from the coupling of the surface

modes of nanotube and nanowire. For the nanocables with a 50 nm radius gold core and 30 nm thick gold cladding, the silica layer D_1 varies in a range of 50 nm-to-300 nm. When the value of D_1 is below 200 nm, the strong coupling between the surface modes of nanotube and nanowire leads to a new characterization of the surface modes, which is shown as a symmetric-like or an antisymmetric-like electromagnetic field distribution. When the silica layer D_1 is large enough, the coupling between them is very weak. Thus the surface modes of nanocable tend to the surface modes of nanotube or nanowire separately. In the following, we plot the electromagnetic field components of the surface modes of nanocable in a strong coupling region ($D_1 = 150$ nm), as well as the coupling process of the electromagnetic fields with various values of D_1. The mathematical form of the electromagnetic fields has been given in expression (1). The angular and the z dependences of all field components are given by S_n and the same for all modes with the same order n. In order to describe the field distribution, it will suffice to evaluate the radial parts from expression (1) which can be viewed as radius-dependent amplitudes along the $z = 0$ and $\phi = 0$ direction.

The electromagnetic field radial distributions of TM_{01} and TM_{02} modes, with frequency ω varying from 1.5 to 5.0 eV, are shown in Fig.11. Only the curves of E_z versus r are plotted for simplicity. For TM_{01} modes in Fig.11(a), the radial distributions of E_z for different frequencies are similar, while the amplitudes of E_z are varying. In Fig.11(b), it is seen that TM_{02} modes below plasmon frequency $\omega = 2.4$ eV are well-behavioured surface modes. At $\omega = 2.4$ eV, TM_{02} modes begin to oscillate in the glass layer and are radiative in the outside air domain. When the frequency increases further, the dispersion curves bend back, the minima of E_z in glass layer decrease and cross zero and the TM_{02} modes transform from surface mode to waveguide mode gradually. The TM_{02} modes with frequencies above 2.8 eV are well-behavioured waveguide modes.

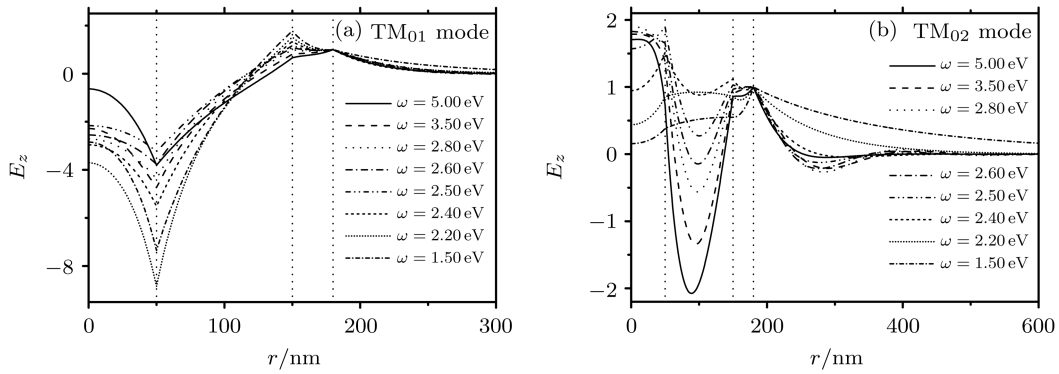


Fig.11. Radial dependence of E_z for TM_{01} mode (a) and TM_{02} mode (b) as a function of radius for different frequencies, with core radius $R_0 = 50$ nm, glass thickness $D_1 = 100$ nm, gold cladding thickness $D_2 = 30$ nm, and $|E_z| = 1$ at the outside gold-air interface chosen for normalization.

In Fig.12, the electromagnetic field components of TM_{01} and TM_{02} modes are plotted as a function of r at $D_1 = 150$ nm. For TM modes, only three components E_r, E_z, H_ϕ are nonzero. Since the angular dependence is $\exp(in\phi)$, for $n = 0$ modes the electromagnetic field is angle independent. In three components, the amplitude of E_z is much larger than those of E_r and H_ϕ. In the outmost air domain, the fields of two modes decay exponentially to zero. For both TM_{01} and TM_{02} modes, the extremes of E_z appear at the interface of two domain, so they are surface modes originating from the coupling of the TM surface modes of gold nanowire and nanotube. At two surfaces of the glass layer, the signs of E_z are opposite for TM_{01}; while, for TM_{02}, they are the same. This behaviour is very similar to those of the anti-symmetric and symmetric surface modes of the symmetric metal-insulator-metal slot structure.[7] Since for TM_{01} mode the E_z curve is antisymmetric-like in the glass layer, while for TM_{02} mode it is symmetric-like, the proportion of electric field of TM_{01} in the glass layer mode is less than that of TM_{02} mode, that is to say, at $D_1 = 150$ nm the TM_{01} mode has a larger loss than TM_{02} mode as shown in Fig.6(b).

The electromagnetic field radial distributions of TM modes with dielectric thickness D_1 varying from 50 to 250 nm are also investigated. As E_z is the dominant field component in TM modes, for simplicity,

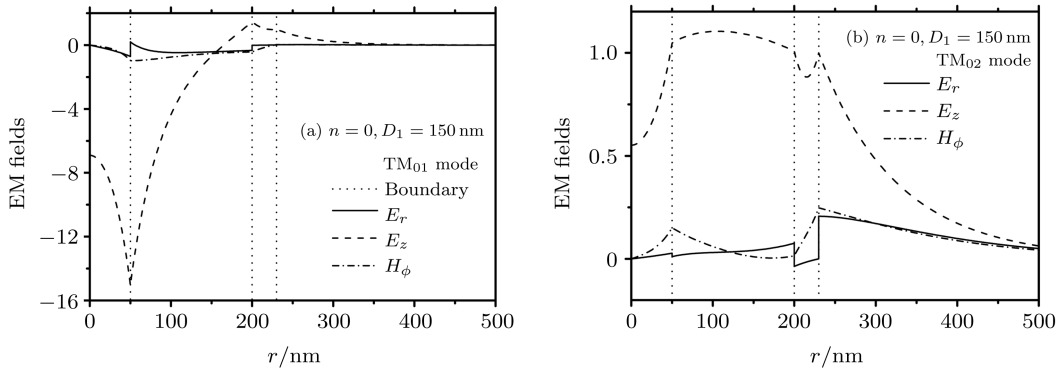


Fig.12. Radial dependence of the field components for TM_{01} mode (a) and TM_{02} mode (b), with wavelength $\lambda = 632.8$ nm, core radius $R_0 = 50$ nm, dielectric thickness $D_1 = 150$ nm, and gold cladding thickness $D_2 = 30$ nm.

only the curves of E_z versus r for TM_{01} and TM_{02} modes are plotted in Fig.13. For the TM_{01} mode, the value of E_z is normalized to unity at the first interface $r = 50$ nm, i.e. metal-silica interface. E_z has an antisymmetric-like distribution due to the strong coupling between two metal domains. While for the TM_{02} mode, the value of E_z is normalized to unity at the second interface, i.e. silica-metal interface. In this case, with the value of D_1 varying from 50 to 250 nm, a symmetric-like E_z distribution is shown in Fig.13(b). It is seen that at $D_1 = 150$ nm, most of the electric field is distributed in the silica layer due to the strong coupling, and it is also corresponding to a long range surface plasmon propagation with a low loss shown in Fig.6(b). When D_1 decreases to zero, the electromagnetic field distribution of TM_{02} mode tends to that of TM surface mode of a gold nanowire with a radius of $R_0 + D_2$. When D_1 is very large, the amplitude of E_z at the inner surface of the gold cladding decreases to zero, and the electromagnetic field distribution of TM_{01} modes tends to that of TM surface mode of gold nanowire with a 50 nm radius; while, for TM_{02} mode, the electromagnetic field distribution tends to that of TM surface mode of gold nanotube with an inner radius of $D_1 + 50$ nm. These trends have also been found in the geometrical dispersion curve of Fig.6.

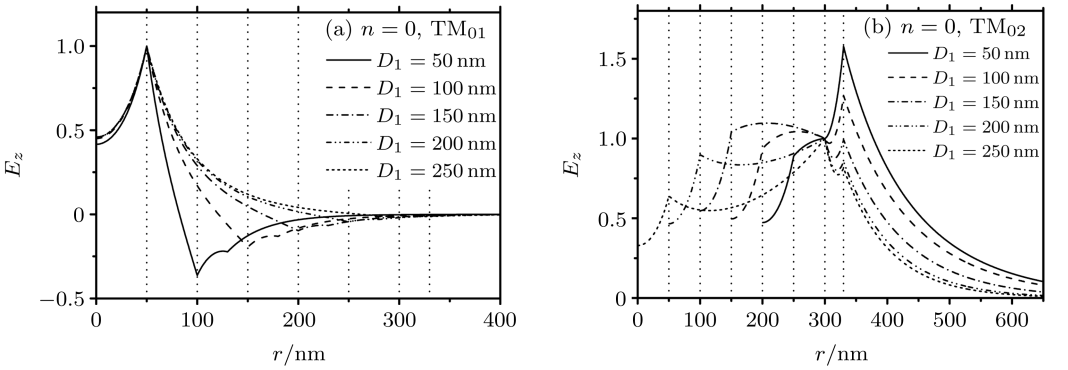


Fig.13. Radial dependence of E_z for TM_{01} mode (a) and TM_{02} mode (b) as a function of radius for different values of dielectric thickness, with wavelength $\lambda = 632.8$ nm, core radius $R_0 = 50$ nm, and gold cladding thickness $D_2 = 30$ nm.

In Fig.14, the electromagnetic fields of two $n = 1$ surface modes are plotted as a function of r at $D_1 = 150$ nm. For $n > 0$, the modes are hybrid and all the six electromagnetic field components are nonzero in general. The amplitudes of electric fields and magnetic fields have about the same order. The extremes of electromagnetic field appear at the interface. These surface modes originate from the coupling of the $n = 1$ surface modes of gold nanowire and nanotube. EH_{11} mode is antisymmetric-like while EH_{12} is symmetric-like. For the same reason that has been analysed, EH_{11} mode has a larger loss than EH_{12} mode in most cases.

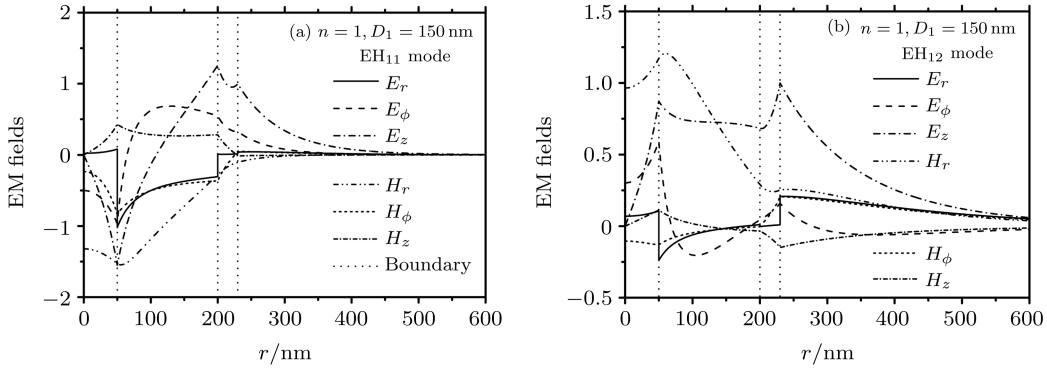


Fig.14. Radial dependence of the field components for EH_{11} mode (a) and EH_{12} mode (b), with wavelength $\lambda = 632.8$ nm, core radius $R_0 = 50$ nm, dielectric thickness $D_1 = 150$ nm, and gold cladding thickness $D_2 = 30$ nm.

The electromagnetic field radial distributions of EH_{11} and EH_{12} modes with the value of dielectric thickness D_1 varying from 50 to 250 nm are shown in Fig.15. With the same normalization, the E_z radial distribution curves of EH_{11} and EH_{12} almost have the same features as what has been found in TM_{01} and TM_{02} modes. E_z for EH_{11} mode has an antisymmetric-like distribution due to the strong coupling between two metal domains. While for EH_{12} mode, with the value of D_1 varying from 50 to 250 nm, a symmetric-like E_z distribution is shown in Fig.15(b). In this region, most of the field is distributed in the silica layer due to the strong coupling and it is corresponding to a long range surface plasmon propagation with a low loss shown in Fig.7(b). When the value of D_1 is large enough, the E_z radial distribution of EH_{11} mode tends to that of the $n = 1$ surface mode of gold nanotube with an inner radius of $D_1 + 50$ nm; while for the EH_{12} mode, the E_z radial distribution tends to that of $n = 1$ surface mode of gold nanowire with a 50 nm radius. When D_1 decreases to zero, EH_{12} mode tends to that of TM surface mode of a gold nanowire with a radius of 50 nm + D_2. These points have also been discussed in the geometrical dispersion curves of Fig.7.

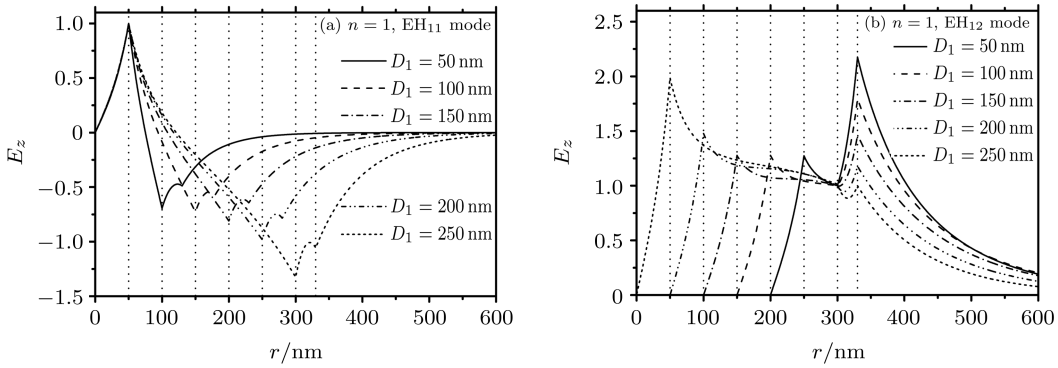


Fig.15. Radial dependence of E_z for EH_{11} mode (a) and EH_{12} mode (b) as a function of radius for different values of dielectric thickness, with wavelength $\lambda = 632.8$ nm, core radius $R_0 = 50$ nm , and gold cladding thickness $D_2 = 30$ nm.

5. Conclusion

We have investigated the surface plasmon polaritons in a lossy gold nanocable theoretically. By solving a complete set of Maxwell's equations in the nanocable, the mode dependences on frequency and geometrical size have been discussed. The coupling between the gold nanocore and nanocladding leads to the symmetric-like and antisymmetric-like surface modes in the nanocable. The mode coupling and transformation between surface modes and waveguide modes have been observed. The results in the weak coupling are compared with the existing theoretical results in nanowire and nanotube.[13] And these results will be helpful for understanding the surface waves in the subwavelength structures.

Acknowledgement

Y. Gu is grateful to Doctors Zhi Li and Zheng Liu and Professor Xiaoyong Hu for their useful discussions.

References

[1] Raether H 1988 *Surface Plasmons* (Berlin: Springer)
[2] Wang X and Cai J H 1993 *Acta Phys. Sin.* **42** 1149 (in Chinese)
[3] Pines D 1956 *Rev. Mod. Phys.* **28** 184
[4] Chen L L, Gu Y and Gong Q H 2007 *Chin. Phys.* **16** 249
[5] Barnes W L, Dereux A and Ebbesen T W 2003 *Nature* **424** 824
[6] Sarid D 1981 *Phys. Rev. Lett.* **47** 1927
[7] Dionne J A, Sweatlock L A, Atwater H A and Polman A 2006 *Phys. Rev.* B **73** 035407
[8] Lamprecht B, Krenn J R, Schider G, Ditlbacher H, Salerno M, Felidj N, Leitner A and Aussenegg F R 2001 *Appl. Phys. Lett.* **79** 1 51
[9] Bozhevolnyi S I, Volkov V S, Devaux E and Ebbesen T W 2005 *Phys. Rev. Lett.* **95** 046802
[10] Miziumski C 1972 *Phys. Lett.* **40**A 187
[11] Pfeiffer C A, Economou E N and Ngai K L 1974 *Phys. Rev.* B **10** 3038
[12] Prade B and Vinet J Y 1994 *J. Lightwave. Tech.* **12** 6
[13] Novotny L and Hafner C 1994 *Phys. Rev.* E **50** 4094
[14] Schröter U and Dereux A 2001 *Phys. Rev.* B **64** 125420
[15] Baida F I, Belkhir A, VanLabeke D and Lamrous O 2006 *Phys. Rev.* B **74** 205419
[16] Stratton J A 1941 *Electromagnetic Theory* (New York: McGraw-Hill)
[17] Jackson J D 1999 *Classical Electrodynamics*, 3rd edn. (New York: Wiley)
[18] Abramowitz M and Stegun I A 1972 *Handbook of Mathematical Functions*, 9th edn. (New York: Dover)
[19] Gillan C J, Schuchinsky A and Spence I 2006 *Comp. Phys. Comm.* **175** 304
[20] Palik E D 1985 *Handbook of Optical Constants of Solids* (Orlando, FL: Academic)
[21] Snyder A W and Love J D 1983 *Optical Waveguide Theory* (New York: Chapman and Hall)
[22] Arakawa E T, Williams M W, Hamm R N and Ritchie R H 1973 *Phys. Rev. Lett.* **31** 1127
[23] Alexander R W, Kovenner G S and Bell R J 1974 *Phys. Rev. Lett.* **32** 154